| OF |
AD A
085 032

END
DATE
FILMED

7-80

DTIC

Some Windows With Very Good Sidelobe Behavior; Application to Discrete Hilbert Transform

Albert H. Nuttall
Surface Ship Sonar Systems Department

9 April 1980

A

NUSC

80 6 4 031

Preface

This research was conducted under NUSC Project No. A75205, Subproject No. ZR0000101, *Applications of Statistical Communication Theory to Acoustic Signal Processing*, Principal Investigator, Dr. A. H. Nuttall (Code 313), Program Manager, J.H. Probus (MAT 08TI), Naval Material Command.

The Technical Reviewer for this report was Dr. G. Clifford Carter (Code 313).

Reviewed and Approved: 9 April 1980

D. Walters
Surface Ship Sonar Systems Department

The author of this report is located at the New London
Laboratory, Naval Underwater Systems Center,
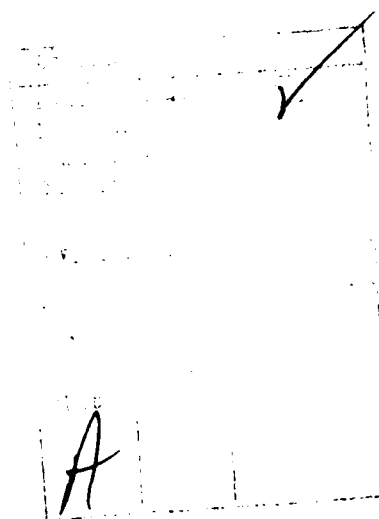New London, Connecticut 06320.

REPORT DOCUMENTATION PAGE		READ INSTRUCTIONS BEFORE COMPLETING FORM
1. REPORT NUMBER TR 6239	2. GOVT ACCESSION NO. *AD-A085 032*	3. RECIPIENT'S CATALOG NUMBER
4. TITLE (and Subtitle) SOME WINDOWS WITH VERY GOOD SIDELOBE BEHAVIOR; APPLICATION TO DISCRETE HILBERT TRANSFORM.		5. TYPE OF REPORT & PERIOD COVERED
		6. PERFORMING ORG. REPORT NUMBER
7. AUTHOR(s) Albert H. Nuttall		8. CONTRACT OR GRANT NUMBER(s)
9. PERFORMING ORGANIZATION NAME AND ADDRESS Naval Underwater Systems Center New London Laboratory New London, CT 06320		10. PROGRAM ELEMENT, PROJECT, TASK AREA & WORK UNIT NUMBERS A75205 ZR0000101
11. CONTROLLING OFFICE NAME AND ADDRESS Naval Material Command MAT 08T1 Washington, DC 20360		12. REPORT DATE 9 April 1980
		13. NUMBER OF PAGES 32
14. MONITORING AGENCY NAME & ADDRESS(if different from Controlling Office)		15. SECURITY CLASS. (of this report) UNCLASSIFIED
		15a. DECLASSIFICATION DOWNGRADING SCHEDULE

16. DISTRIBUTION STATEMENT (of this Report)

Approved for public release; distribution unlimited.

17. DISTRIBUTION STATEMENT (of the abstract entered in Block 20, if different from Report)

18. SUPPLEMENTARY NOTES

19. KEY WORDS (Continue on reverse side if necessary and identify by block number)

Analytic Waveform	Weighted Overlap Processing
Asymptotic Decay of Sidelobes	Weightings
Bias	Windows
Discrete Hilbert Transform	Discrete Fourier Series
Sidelobes	

20. ABSTRACT (Continue on reverse side if necessary and identify by block number)

Some of the windows presented by Harris, Proc. IEEE, Jan. 78, are not correct in terms of their reported peak sidelobes and optimal behavior. We present corrected plots of Harris' windows and also derive additional windows with very good sidelobes and optimal behavior under several different constraints. These plots enable the reader to select a window to suit his require-

DD $_{1\ JAN\ 73}^{FORM}$ 1473 EDITION OF 1 NOV 65 IS OBSOLETE
S/N 0102-014-6601

20. (continued)

ments, in terms of bias due to near-by sidelobes and bias due to distant sidelobes. An application of the new windows to a technique for calculating the discrete Hilbert transform is presented.

TABLE OF CONTENTS

LIST OF ILLUSTRATIONS

LIST OF TABLES

SOME WINDOWS WITH VERY GOOD
SIDELOBE BEHAVIOR;
APPLICATION TO DISCRETE
HILBERT TRANSFORM

INTRODUCTION

The use of temporal weightings for spectral analysis, with good sidelobe behavior and small bias, is well established and documented in Harris (ref. 1). However, some of the plots of the spectral windows are not correct and do not have the optimal sidelobe levels claimed. We will present the corrected plots and some additional windows with optimal properties. Finally, some of these results will be applied to obtain a discrete Hilbert transform.

The temporal weightings considered will be continuous functions of time (except possibly at $t = \pm L/2$) and duration L; i.e.,

$$w(t) = 0 \quad \text{for} \quad |t| > L/2 .\tag{1}$$

The Fourier transform of the temporal weighting is the spectral window

$$W(f) = \int_{-L/2}^{L/2} dt \, w(t) \exp(-i2\pi ft)\tag{2}$$

and is a continuous function of frequency, defined for all f. Notice the notational convention adopted here: a weighting is applied multiplicatively in one domain, and its Fourier-transform (called a window) occurs as a convolution in the other domain.

All the window results presented here are obtained by exact analytical evaluation of (2) and are valid for all values of f. However, window (2) can be approximately evaluated at any f, by means of some numerical integration rule (such as Trapezoidal), by choosing increment $\Delta = L/M$, where M is a large integer. These latter results are not adequate for $| f | > .5/\Delta$, because the approximation yielded by this numerical integration procedure has period $1/\Delta$ in f. Furthermore, if we limit the frequencies f, at which this numerical evaluation is conducted, to the values $n/(N\Delta)$ (for n and N integer), the results can be realized as an N-point discrete Fourier transform (DFT). Since the frequency spacing at which these values occur is $(N\Delta)^{-1}$ and the width of the spectral window (2) is of the order $1/L = (M\Delta)^{-1}$, we would also require $N>M$ if we desire to observe fairly closely the changes in the window (2) by means of an N-point DFT. There is no fundamental restriction on the relative sizes of M and N; however, M must be large in order to obtain an accurate approximation to (2).

GENERAL WEIGHTING CONSIDERATIONS

The temporal weightings of interest here are of the form

$$w(t) = \frac{1}{L} \sum_{k=0}^{K} a_k \cos(2\pi k t/L) \quad \text{for} \quad |t| \leqslant L/2, \tag{3}$$

where $\{a_k\}_0^K$ are real constants. The weighting is symmetric about $t = 0$ and possesses all orders of derivatives for $|t| < L/2$; however, discontinuities in $w(t)$, defined by (1) and (3), or in its derivatives, occur at $t = \pm L/2$. These discontinuities dictate the asymptotic behavior for large $|f|$ of $W(f)$ in (2). Without loss of generality, the weighting is normalized according to

$$\sum_{k=0}^{K} a_k = 1; \qquad w(0) = \frac{1}{L} \sum_{k=0}^{K} a_k = \frac{1}{L}. \tag{4}$$

Observe from (3) that

$$w(\pm \frac{L}{2}) = \lim_{|t| \to L/2-} w(t) = \frac{1}{L} \sum_{k=0}^{K} (-1)^k a_k, \tag{5}$$

which may or may not be equal to zero. If (5) is not zero, then weighting $w(t)$ is discontinuous at $t = \pm L/2$, and window $W(f)$ will decay only as $1/f$ for large $|f|$.

However, if (5) is zero, then $w(t)$ is continuous for all t. Also, $w'(t)$ is continuous for all t, since we always have

$$w'(t) = -\frac{2\pi}{L^2} \sum_{k=0}^{K} k a_k \sin(2\pi k t/L) \quad \text{for} \quad |t| < L/2, \tag{6}$$

and

$$\lim_{|t| \to L/2-} w'(t) = 0; \qquad w'(t) = 0 \quad \text{for} \quad |t| > L/2. \tag{7}$$

The last property follows from (1). Thus, when weighting values $w(\pm L/2)$ in (5) are zero, $w(t)$ and $w'(t)$ are both continuous for all t.

However, $w''(t)$ may then not be continuous at $t = \pm L/2$. We have from (6),

$$w''(t) = -\frac{4\pi^2}{L^3} \sum_{k=0}^{K} k^2 a_k \cos(2\pi k t/L) \quad \text{for} \quad |t| < L/2 \tag{8}$$

and

$$\lim_{|t| \to L/2-} w''(t) = -\frac{4\pi^2}{L^3} \sum_{k=0}^{K} (-1)^k k^2 a_k, \tag{9}$$

which may or may not be zero. If (9) is not zero, then $w''(t)$ is discontinuous at $t = \pm L/2$, and $W(f)$ will decay as $1/f^3$ for large $|f|$.

Conversely, if (9) is zero, then $w''(t)$ is continuous for all t, and it follows (similarly to above) that $w'''(t)$ is continuous for all t. Then $W(f)$ decays at least as fast as $1/f^5$ for large $|f|$. We will have occasion to use these relations later.

The spectral window corresponding to $w(t)$ in (1) and (3) is given by (2) as the closed form expression

$$W(f) = \frac{Lf}{\pi} \sin(\pi Lf) \sum_{k=0}^{K} \frac{(-1)^k a_k}{L^2 f^2 - k^2} \quad \text{for all } f;$$

$$W(n/L) = \begin{Bmatrix} a_0, n=0 \\ \frac{1}{2} a_{|n|}, n \neq 0 \end{Bmatrix} \quad . \tag{10A}$$

If we expand $(L^2 f^2 - k^2)^{-1}$ in a power series in $\left(\frac{k}{Lf}\right)^2$, we obtain

$$W(f) = \frac{\sin(\pi L f)}{\pi L f} \sum_{m=0}^{\infty} \frac{1}{(Lf)^{2m}} \sum_{k=0}^{K} (-1)^k k^{2m} a_k \quad \text{for} \quad |Lf| > K \ . \tag{10B}$$

Thus, the quantities (5) and (9) considered above are simply the $m=0$ and $m=1$ coefficients of this expansion; the asymptotic behavior of (10B) depends on the first non-zero term in the m-series, and will be plotted in the following figures as a dotted line.

DISCRETE FOURIER SERIES

When continuous temporal weighting is used in digital processing, it is sampled and often transformed into the frequency domain, where its effect can be included as a convolution of its discrete Fourier series with the data DFT. To evaluate this discrete Fourier series, we begin by delaying the temporal weight to the interval (0,L):

$$
w_D(t) \equiv w\left(t - \frac{L}{2}\right) = \frac{1}{L} \sum_{k=0}^{K} (-1)^k a_k \cos(2\pi kt/L)
$$
$$
= \frac{1}{L} \sum_{k=-K}^{K} (-1)^k \varepsilon_k a_{|k|} \exp(i2\pi kt/L) \quad \text{for} \quad 0 \leqslant t \leqslant L,
$$
(11)

where

$$
\varepsilon_k = \begin{Bmatrix} 1, & k = 0 \\ \tfrac{1}{2}, & k \neq 0 \end{Bmatrix} .
$$
(12)

Let the sampling interval on weighting $w_D(t)$ be

$$
\Delta = L/M ,
$$
(13)

where M is even; then samples (temporal weights)

$$
w_D(m\Delta) = \frac{1}{L} \sum_{k=-K}^{K} (-1)^k \varepsilon_k a_{|k|} \exp(i2\pi km/M) \quad \text{for} \quad 0 \leqslant m \leqslant M .
$$
(14)

Then for M>2K, the discrete Fourier series is given by the M-point DFT (ref. 2, ch. 3)*

$$
\sum_{m=0}^{M-1} \Delta w_D(m\Delta) \exp(-i2\pi mn/M) = (-1)^n \varepsilon_n a_{|n|} \quad \text{for} \quad |n| \leqslant M/2 .
$$
(15A)

Thus, the effects of temporal weighting (14) can be incorporated in a digital processing application as a frequency convolution of the data DFT with the sequence

$$
\dots, 0, 0, (-1)^K \frac{1}{2} a_K, \dots, -\frac{1}{2} a_1, a_0, -\frac{1}{2} a_1, \dots, (-1)^K \frac{1}{2} a_K, 0, 0, \dots .
$$
(15B)

This is one of the main reasons for employing weightings of the form (14) in digital processing applications; namely, the effects of temporal weighting are easily in-

---

* This consideration is different from that mentioned under (2),where we were interested in approximately evaluating window W(f) in (2) by means of a DFT.

cluded by means of convolution in the discrete frequency domain with a short sequence of length $2K + 1$.

The effect of sampling continuous weighting $w(t)$ at increment Δ, in so far as the effective window is concerned, is as follows. The effective window is*

$$W_e(f) = \int dt\, \Delta\delta_\Delta(t)\, w(t)\, \exp(-i2\pi ft)$$

$$= \delta_{\frac{1}{\Delta}}(f) \circledast W(f) = \sum_{n=-\infty}^{\infty} W(f - \frac{n}{\Delta}) , \tag{16}$$

where $\delta_a(x)$ is an infinite unit-area impulse train in x at spacing a. Thus there are periodic replications in $W_e(f)$ at multiples of $1/\Delta$; the aliasing at $f = \pm .5/\Delta$ is obvious. All the following results correspond to $\Delta = 0$, i.e., continuous weightings; thus, there is no aliasing.

---

* Integrals without limits are over the range of non-zero integrand.

HARRIS' WINDOWS

The first weighting to be considered is Hanning, for which there are only two non-zero coefficients in (3):

$$a_0 = .5, \quad a_1 = .5, \quad W(f) = \frac{\sin(\pi Lf)}{2\pi Lf(1-L^2f^2)} \quad . \tag{17}$$

Its power response in dB is plotted versus Lf in figure 1, normalized to the peak response at $f = 0$; that is

$$dB \equiv 10 \log|W(f)/W(0)|^2 \tag{18}$$

is plotted.* The largest sidelobe is -31.47 dB. Since (5) is zero for the weights in (17), but (9) is not, the Hanning window has an asymptotic decay of 18 dB/octave; this decay is the first non-zero term in (10B).

The second weighting is Blackman (ref. 1, eq. 32):

$$a_0 = .42, \quad a_1 = .50, \quad a_2 = .08 \quad . \tag{19}$$

The window is depicted in figure 2. Again, (5) is zero, but (9) is not; thus the asymptotic decay is 18 dB/octave. The largest sidelobe is -58.11 dB.

The "exact" Blackman weights are (ref. 1, p. 63)

$$a_0 = 7938/18608, \quad a_1 = 9240/18608, \quad a_2 = 1430/18608 \quad . \tag{20}$$

Now (5) is not zero; therefore, the window decays at only 6 dB/octave as shown in figure 3. However, the largest sidelobe is -68.24 dB, not -51 dB as cited in ref. 1, fig. 23. Also, the sidelobes in figure 3 are about 6 dB lower than those reported in ref. 1, fig. 23.

The following four windows are listed in the table on page 65 of ref. 1. The "minimum" 3-term weights are

$$a_0 = .42323, \quad a_1 = .49755, \quad a_2 = .07922 \quad . \tag{21}$$

Since (5) is not zero, the window decay is only 6 dB/octave, as shown in figure 4. The maximum sidelobe is -70.83 dB, not -67 dB as reported in ref. 1, figure 24 and page 64.

---

* When the weighting is applied instead in the lag domain, as for Blackman-Tukey spectral analysis, rather than in the time domain as presumed here, the window appears linearly rather than as its square. In this case, the square must be removed from the definition in (18), and all the plots require that the dB numbers on the ordinate be halved. For example, the peak Hanning sidelobe is then -15.73 dB.

The 3-term weights are

$$a_0 = .44959, \quad a_1 = .49364, \quad a_2 = .05677 . \tag{22}$$

The corresponding window is given in figure 5 and has a maximum sidelobe of −62.05 dB, rather than the −61 dB reported in ref. 1, p. 65. Since (5) is not zero, the decay is only at 6 dB/octave, as indicated by the dotted line.

The "minimum" 4-term weights are*

$$a_0 = .35875, \quad a_1 = .48829, \quad a_2 = .14128, \quad a_3 = .01168 . \tag{23}$$

Although (5) is not zero, it is nearly so. Therefore, the initial decay of the window is greater than 6 dB/octave; however, it must eventually decay only as 6 dB/octave. The maximum sidelobe of the window is indicated in figure 6; it is −92 dB, as reported in ref. 1.

The 4-term weights are

$$a_0 = .40217, \quad a_1 = .49703, \quad a_2 = .09892, \quad a_3 = .00188 . \tag{24}$$

The asymptotic decay is only 6 dB/octave, as shown in figure 7, and the largest sidelobe is −74.39 dB, as claimed in ref. 1, p. 65.

---

* These are not the weights actually listed in ref. 1, page 65. However, the values listed there do not add up to 1; accordingly, we have modified them according to the comment under eq. 34, and made them sum to 1 (with the lowest sidelobe possible by modifying just one of the last digits).
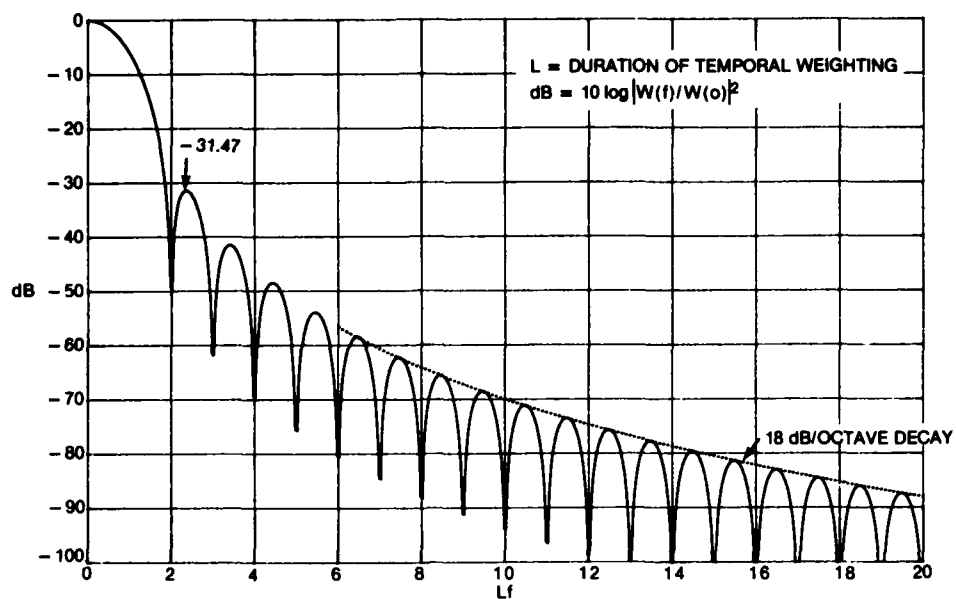
Figure 1. Hanning Window for $a_0 = .5$, $a_1 = .5$
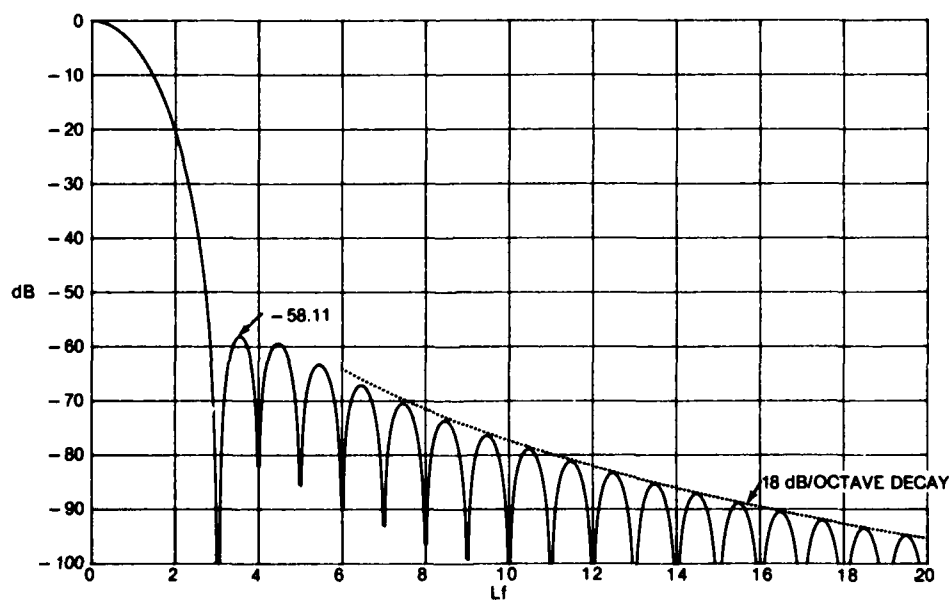
Figure 2. Blackman Window for $a_0 = .42$, $a_1 = .5$, $a_2 = .08$
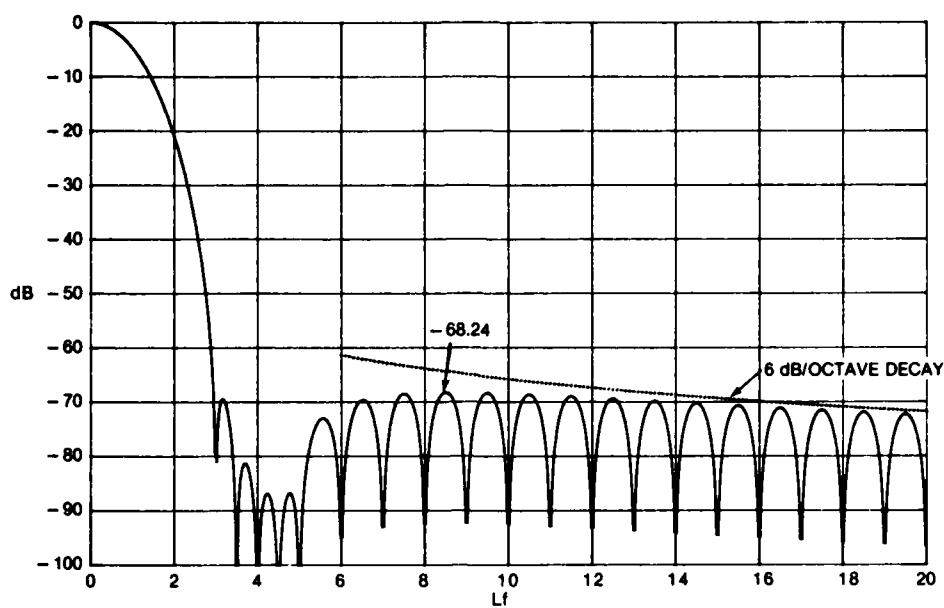
Figure 3. Exact Blackman Window for $a_0 = 7938/18608$, $a_1 = 9240/18608$, $a_2 = 1430/18608$
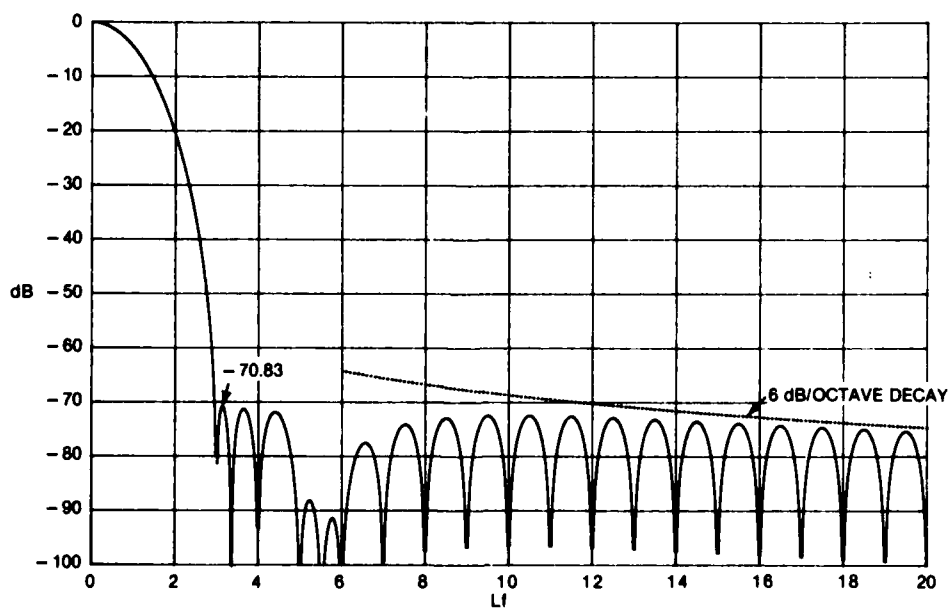
Figure 4. "Minimum" 3-Term Window for $a_0 = .42323$, $a_1 = .49755$, $a_2 = .07922$
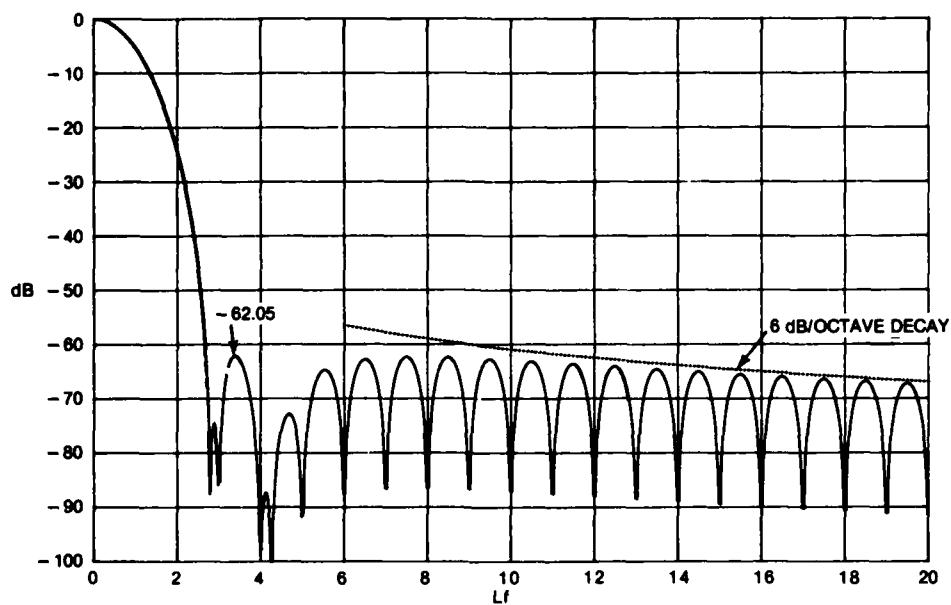
Figure 5. 3-Term Window for $a_0 = .44959$, $a_1 = .49364$, $a_2 = .05677$
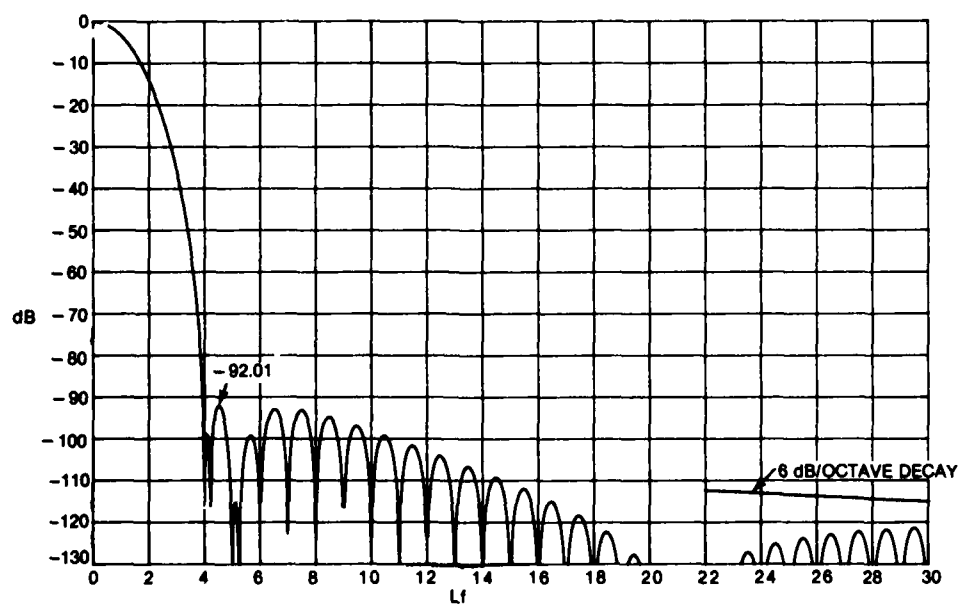
Figure 6. "Minimum" 4-Term Window for $a_0 = .35875$, $a_1 = .48829$,
$a_2 = .14128$, $a_3 = .01168$
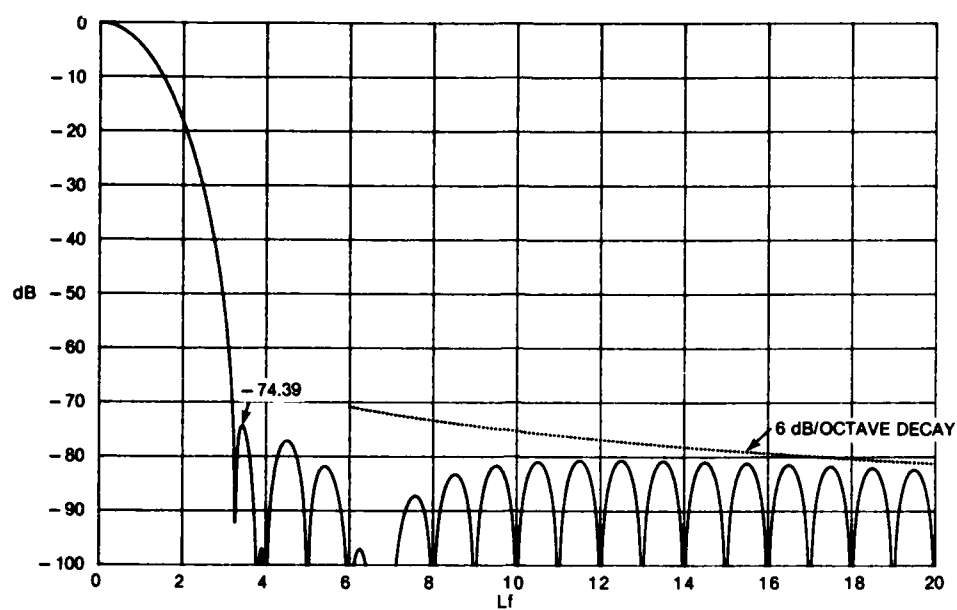
Figure 7. 4-Term Window for $a_0 = .40217$, $a_1 = .49703$, $a_2 = .09892$, $a_3 = .00188$

RAPIDLY DECAYING WINDOWS WITH MINIMAL SIDELOBES

It was observed earlier that the window W(f) decays fairly rapidly for large f if (5) is zero, and very rapidly if (9) is zero. Such windows will lead to spectral estimates that are immune to strong interferences at frequencies removed from those of interest. In this section, we will consider this class of windows in terms of the peak sidelobe and asymptotic decay; the mainlobe width of each window is not discussed, but is easily determined from the plots. Discontinuous weightings will be taken up later.

If only two coefficients in weighting (3) are non-zero, satisfaction of (4), and setting (5) equal to zero, yield

$$a_0 + a_1 = 1, \quad a_0 - a_1 = 0 . \tag{25}$$

The Hanning window satisfies these requirements and is plotted in figure 1. Convolution sequence (15B) is simply $-1/4, 1/2, -1/4$.

Moving on to three non-zero coefficients in (3), if we satisfy (4), and set (5) and (9) equal to zero, we find

$$a_0 = 3/8, \quad a_1 = 4/8, \quad a_2 = 1/8 . \tag{26}$$

The weighting is

$$w(t) = \frac{1}{L} \cos^4(\pi t / L) \quad \text{for} \quad |t| \leqslant L/2 . \tag{27}$$

From (15B), the discrete Fourier series for convolution is

$$\frac{1, -4, 6, -4, 1}{16} , \tag{28}$$

which are simply the binomial coefficients. As noted under (9), since the third derivative of w(t) is continuous at $t = \pm L/2$, the window decays at a 30 dB/octave rate. The plot in figure 8 indicates that the largest sidelobe is -46.74 dB.

Instead of forcing (9) equal to zero, we can use the one degree of freedom left, after (4) is satisfied and (5) is set equal to zero, to minimize the maximum sidelobes. The optimal weights are found to

$$a_0 = .40897, \quad a_1 = .5, \quad a_2 = .09103 . \tag{29}$$

The corresponding window is presented in figure 9. The asymptotic decay is 18 dB/octave, and the two equal sidelobes are of size -64.19 dB. This is 6.1 dB better than the -58.1 dB sidelobe of the Blackman window, yet the asymptotic decays are equal. Although the maximum sidelobe of the "minimum" 3-term window in figure 4 is 6.6 dB better, that decay is only 6 dB/octave rather than the 18 dB/octave decay here.

When we consider four non-zero coefficients in (3), we have several alternatives. If we satisfy (4), set (5) and (9) both equal to zero, and also set the fourth derivative of $w(t)$ equal to zero at $t = \pm L/2$, we have four equations in four unknowns, with solution

$$a_0, a_1, a_2, a_3 = \frac{10, 15, 6, 1}{32} \ . \tag{30}$$

The weighting is

$$w(t) = \frac{1}{L} \cos^6(\pi t/L) \quad \text{for} \quad |t| \leqslant \frac{L}{2}, \tag{31}$$

and from (15B), the discrete Fourier series for convolution is

$$\frac{-1, 6, -15, 20, -15, 6, -1}{64}, \tag{32}$$

which are again the binomial coefficients. The window decays at a very fast rate of 42 dB/octave, since the fifth derivative of $w(t)$ is continuous for all t. The plot in figure 10 shows the maximum sidelobe to be -60.95 dB.

If we satisfy (4), and set (5) and (9) both equal to zero, but use the remaining degree of freedom to minimize the maximum sidelobes, the optimal weights are determined to be

$$a_0 = .338946, \quad a_1 = .481973, \quad a_2 = .161054, \quad a_3 = .018027 \ . \tag{33}$$

The window is given in figure 11 and has two equal sidelobes of -82.60 dB. The asymptotic decay is 30 dB/octave, since the third derivative of $w(t)$ is continuous for all t. Comparison with the "minimum" 4-term window in figure 6 reveals a difference of 9.4 dB in the maximum sidelobe; however, the decay of figure 11 is much faster at a 30 dB/octave rate. As far as the 4-term window in figure 7 is concerned, figure 11 has an 8.2 dB better maximum sidelobe and a much better decay, 30 dB/octave versus 6 dB/octave.

Finally, if we satisfy (4), and set only (5) equal to zero, and use the remaining two degrees of freedom to minimize the maximum sidelobes, the optimal weights are found to be

$$a_0 = .355768, \quad a_1 = .487396, \quad a_2 = .144232, \quad a_3 = .012604 \ . \tag{34}$$

The window is shown in figure 12 and has three equal sidelobes of -93.32 dB. Notice that this level is better than the purported "minimum" 4-term level of -92 dB claimed in ref. 1, pp. 64-65; and the asymptotic decay is 18 dB/octave, not 6 dB/octave. Furthermore, this level was achieved under the constraint of setting (5) equal to zero. If we were to eliminate this constraint of a continuous weighting function, a sidelobe level lower than -93.32 dB can be achieved. (This problem and

the determination of the true minimum 3-term window (to replace figure 4) are undertaken in the next section.) Comparison with the 4-term window of figure 7 reveals an 18.9 dB peak-sidelobe improvement in figure 12 and a better decay of 18 dB/octave instead of 6 dB/octave.
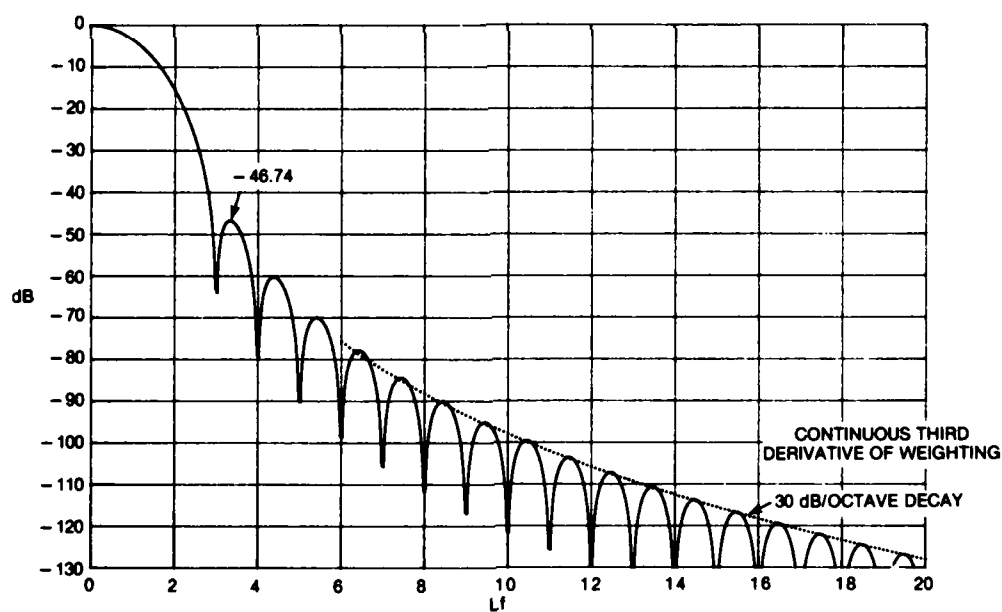

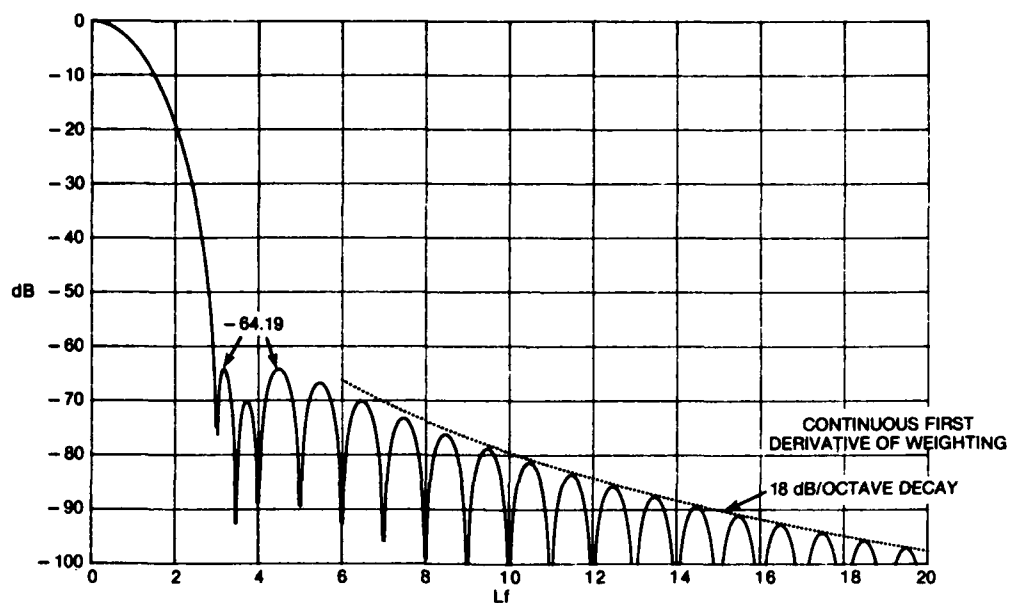Figure 8. Window for $a_0 = .375$, $a_1 = .5$, $a_2 = .125$

Figure 9. Window for $a_0 = .40897$, $a_1 = .5$, $a_2 = .09103$
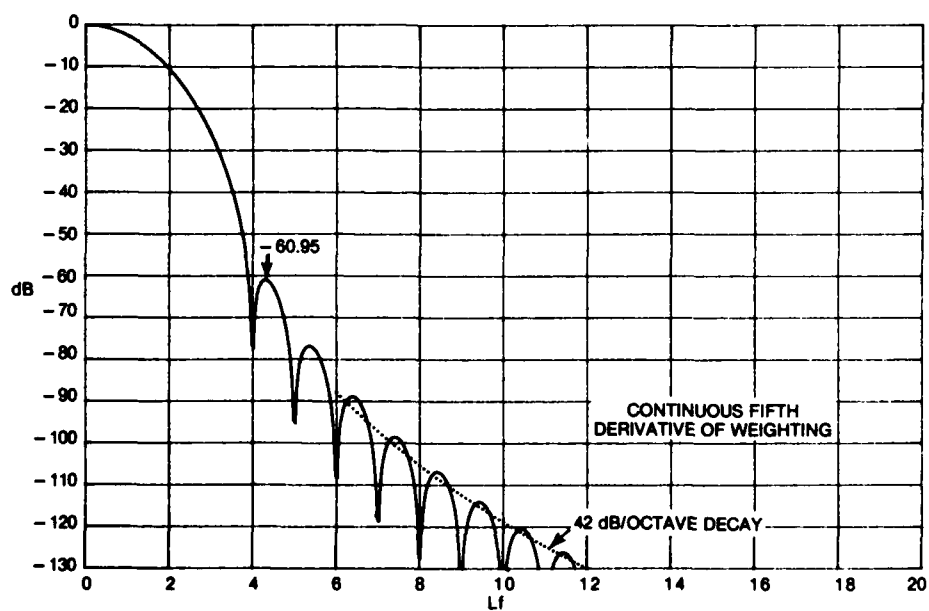
Figure 10. Window for $a_0 = 10/32$, $a_1 = 15/32$, $a_2 = 6/32$ $a_3 = 1/32$
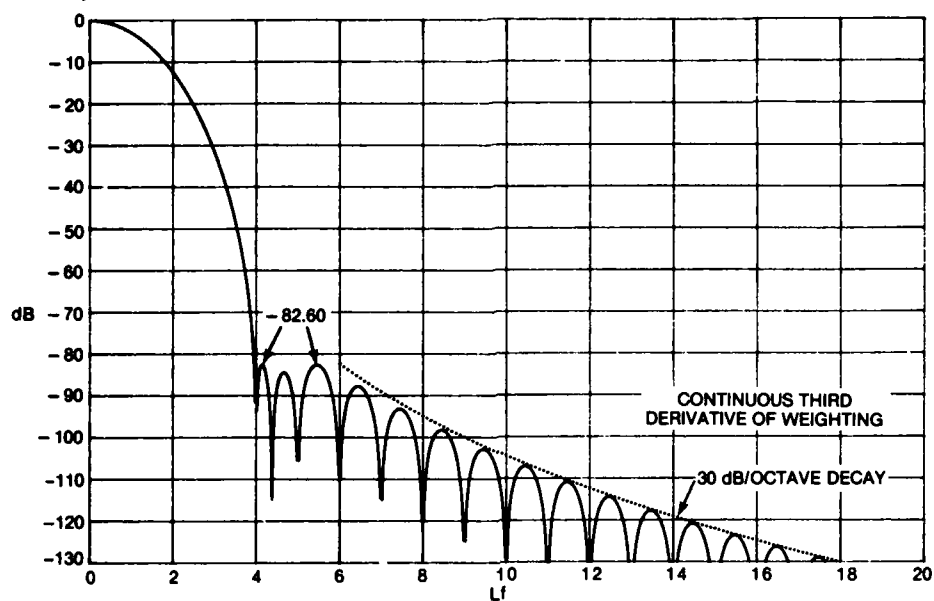
Figure 11. Window for $a_0 = .338946$, $a_1 = .481973$, $a_2 = .161054$, $a_3 = .018027$
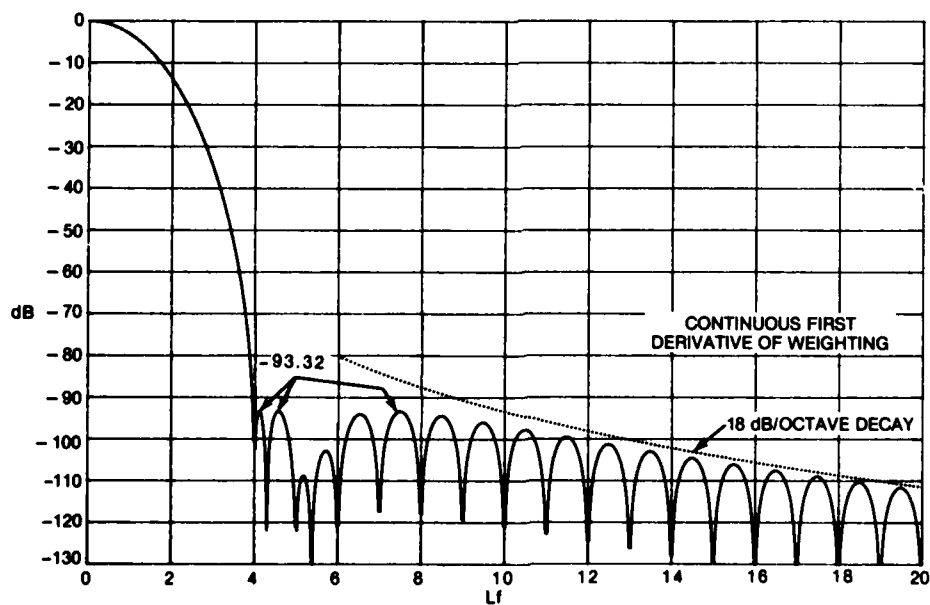
Figure 12. Window for $a_0 = .355768$, $a_1 = .487396$, $a_2 = .144232$, $a_3 = .012604$

MINIMUM SIDELOBE WINDOWS

If only two coefficients in weighting (3) are non-zero, and we disregard the continuity requirement (5), the one degree of freedom left, after normalization (4) is satisfied, can be used to minimize the maximum sidelobes. The result is the familiar Hamming window, plotted in figure 13, with coefficients

$$a_0 = .53836, \quad a_1 = .46164 . \tag{35}$$

The two equal peak-sidelobes are -43.19 dB, and the asymptotic decay is only 6 dB/octave, as dictated by (10B) when (5) is not zero.

For three non-zero coefficients in (3), satisfaction of (4) leaves two degrees of freedom. These can be used to realize the minimum 3-term window in figure 14, for which the optimal coefficients are

$$a_0 = .4243801, \quad a_1 = .4973406, \quad a_2 = .0782793 . \tag{36}$$

There are three equal peak-sidelobes of -71.48 dB, which is .65 dB better than figure 4, with an asymptotic decay of 6 dB/octave for both.

When four coefficients are non-zero in (3), there are three degrees of freedom left after normalization (4). The minimum 4-term window results for coefficients

$$a_0 = .3635819, \quad a_1 = .4891775, \quad a_2 = .1365995, \quad a_3 = .0106411 , \tag{37}$$

and is shown in figure 15. The four equal sidelobes are at level -98.17 dB, which is 6.16 dB better than figure 6, with an asymptotic decay of 6 dB/octave for both. This sidelobe level is 4.85 dB better than figure 12, but the decay in figure 12 is 18 dB/octave.

Figure 13. Hamming Window for $a_0 = .53836$, $a_1 = .46164$
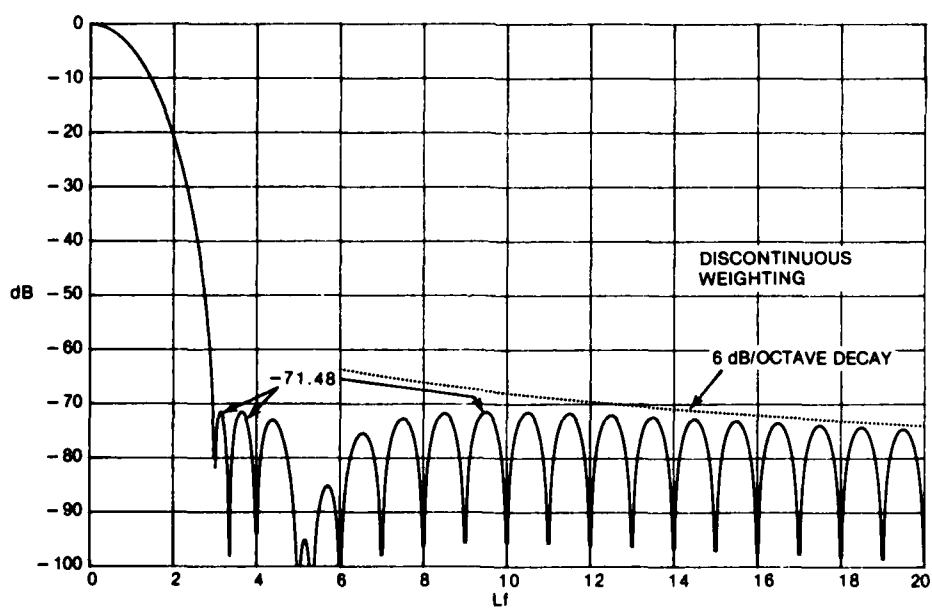
Figure 14. Minimum 3-Term Window for $a_0 = .4243801$, $a_1 = .4973406$, $a_2 = .0782793$

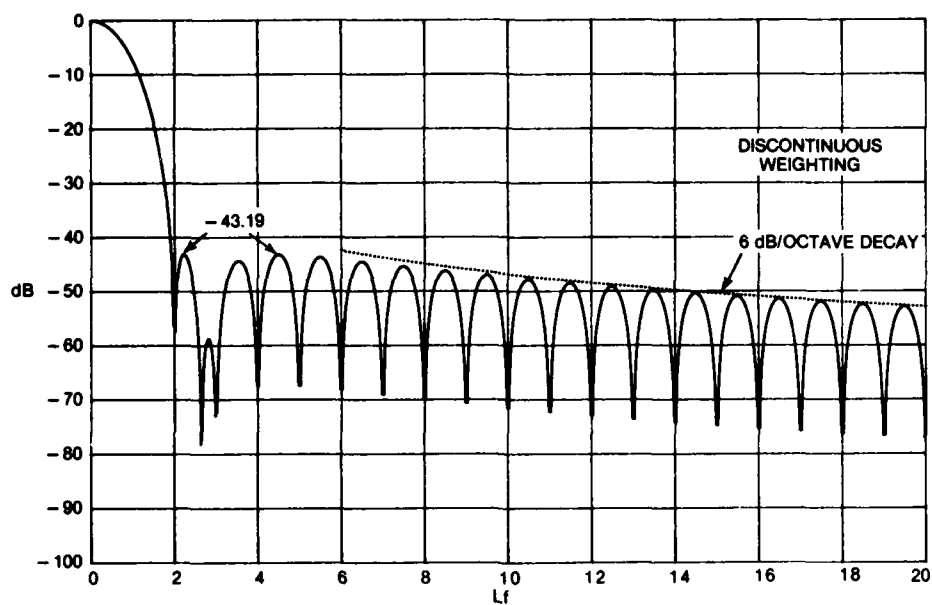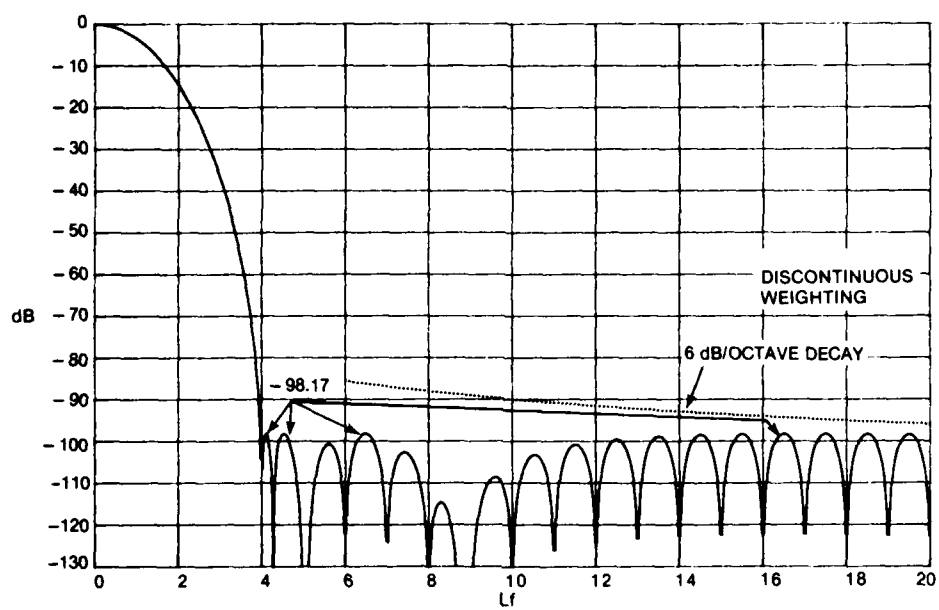Figure 15. Minimum 4-Term Window for $a_0 = .3635819$, $a_1 = .4891775$, $a_2 = .1365995$, $a_3 = .0106411$

COMPARISON WITH KAISER-BESSEL AND VAN DER MAAS WINDOWS

The windows in figures 13, 14, and 15 are very similar to the Kaiser-Bessel window. Specifically, the Kaiser-Bessel weighting and window are

$$w(t) = \frac{1}{L} \, I_0 \left(B\sqrt{1 - (2t/L)^2} \right) \quad \text{for} \quad |t| < L/2 ,$$

$$W(f) = \frac{\sin \left(\sqrt{\pi^2 L^2 f^2 - B^2} \right)}{\sqrt{\pi^2 L^2 f^2 - B^2}} \quad \text{for all } f, \tag{38}$$

respectively, where B is a parameter. If we choose B to make the first null of the Kaiser-Bessel window lie at the three alternatives of $Lf = 2,3,4$ (as in figures 13, 14, and 15, respectively), we obtain the plots in figures 16, 17, and 18. The corresponding mainlobe shapes are indistinguishable, and the asymptotic decays are all 6 dB/octave. The immediate sidelobes of the Kaiser-Bessel windows are several dB larger than the minimum results in figures 13, 14, and 15, but the distant sidelobes of the Kaiser-Bessel windows are over 10 dB lower for the examples considered. Thus, a trade-off exists between the peak sidelobe and the distant sidelobe level.

The windows here are also similar to the ideal impulsive van der Maas window given by

$$w(t) = \frac{B}{L} \, \frac{I_1 \left(B\sqrt{1 - (2t/L)^2} \right)}{\sqrt{1 - (2t/L)^2}} + \frac{1}{2} \, \delta \left(t - \frac{L}{2} \right) + \frac{1}{2} \, \delta \left(t + \frac{L}{2} \right) \quad \text{for } |t| \leqslant \frac{L}{2} ,$$

$$W(f) = \cos \left(\sqrt{(\pi L f)^2 - B^2} \right) \quad \text{for all } f . \tag{39}$$

This window is characterized by having the narrowest possible mainlobe width for a specified sidelobe level, and vice versa. However, the window does not decay at all for large f. The peak to sidelobe voltage level is $SL \equiv \cosh(B)$, and the first null of the window occurs at

$$Lf_0 = \left(\frac{1}{4} + \frac{B^2}{\pi^2} \right)^{1/2} . \tag{40}$$

Thus, the first null location can be expressed in terms of the sidelobe level SL according to

$$Lf_0 = \left(\frac{1}{4} + \left[\frac{\ln \left(SL + \sqrt{SL^2 - 1} \right)}{\pi} \right]^2 \right)^{1/2} . \tag{41}$$

Table 1 shows this null location and the actual location for several of the windows presented earlier, when the peak sidelobes are equal; the agreement is close, especially for those windows with a 6 dB/octave decay, figures 13, 14, and 15.

Table 1. Comparison of Null Location with van der Maas Case

Figure Number	Null Location	van der Maas Null Location
9	3	2.62
11	4	3.29
12	4	3.67
13	2	1.87
14	3	2.88
15	4	3.85
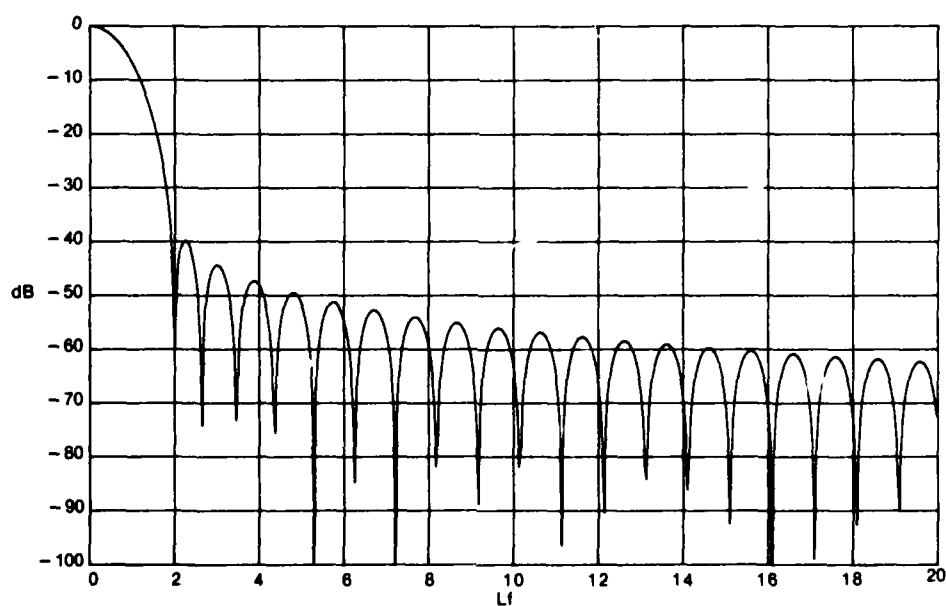
Figure 16. Kaiser-Bessel Window with First Null at Lf = 2

21
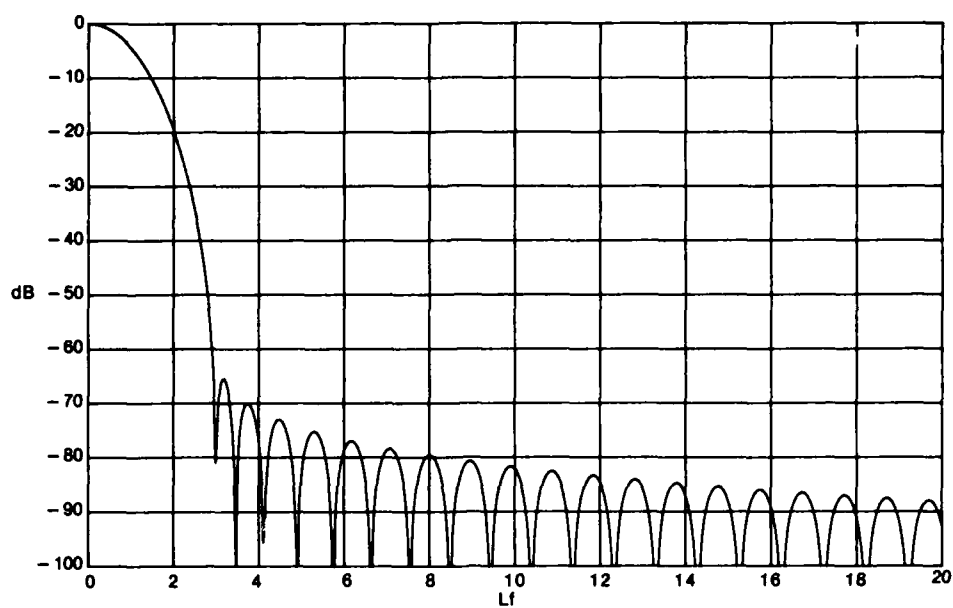
Figure 17. Kaiser-Bessel Window with First Null at Lf = 3
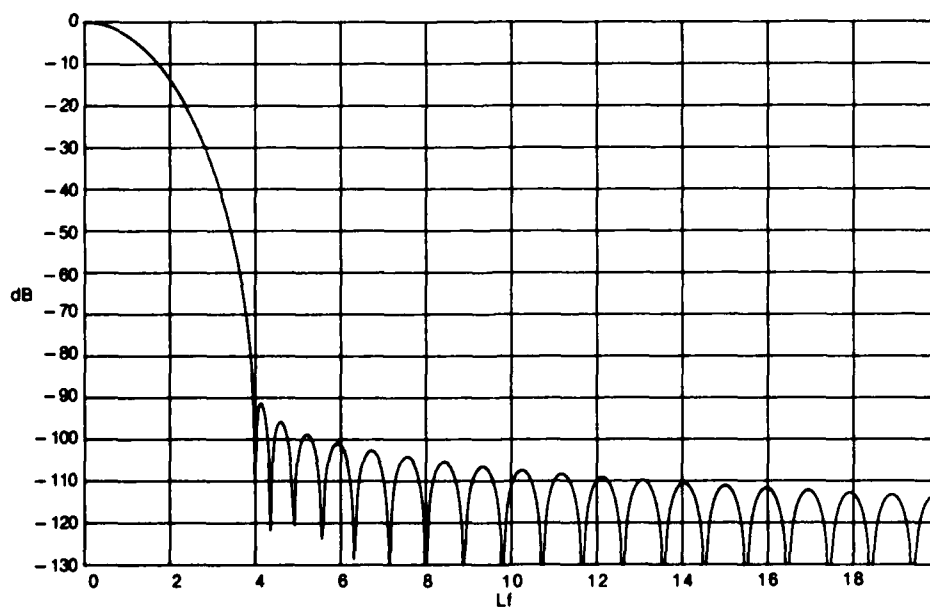
Figure 18. Kaiser-Bessel Window with First Null at Lf = 4

DISCRETE HILBERT TRANSFORM

For a continuous-time real waveform x(t), the (voltage-density) spectrum

$$X(f) = \int dt \, x(t) \exp(-i2\pi ft) \tag{42}$$

is conjugate symmetric about $f = 0$; i.e., $X(-f) = X^*(f)$. If we suppress the negative-frequency components and double the positive-frequency components, we obtain the analytic waveform:

$$X_+(f) = [1 + \text{sgn}(f)] X(f), \tag{43}$$

and

$$x_+(t) = x(t) + ix_H(t). \tag{44}$$

Here $x_H(t)$ is the Hilbert transform of $x(t)$:

$$x_H(t) = \frac{1}{\pi t} \circledast x(t) = \frac{1}{\pi} \int d\tau \, \frac{x(\tau)}{t-\tau}. \tag{45}$$

When we consider instead a discrete-time real waveform with samples occurring every Δ seconds, the spectrum has period $1/\Delta$, and the discrete Hilbert transform (DHT) takes another form (ref. 2, ch. 7). Specifically, the Fourier coefficients of an N-point DFT of the waveform samples are multiplied by the sequence $\{u_n\}_0^{N-1}$, where (ref. 2, p. 354)

$$u_n = \begin{cases} 1, & n = 0 \text{ and } n = N/2 \\ 2, & 0 < n < N/2 \\ 0, & N/2 < n \leqslant N-1 \end{cases}. \tag{46}$$

However, this ideal characteristic exists only in a theoretical sense; its effect must be approximated in practice (ref. 2, p. 361).

A method of obtaining an accurate DHT for long data sequences is now presented. We begin by considering a continuous cosine wave at frequency f_0:

$$x(t) = A \cos(2\pi f_0 t + \theta). \tag{47}$$

The spectrum of this waveform, from the infinite transform (42), is a pair of impulses:

$$X(f) = \frac{A}{2} \exp(i\theta) \delta(f-f_0) + \frac{A}{2} \exp(-i\theta) \delta(f+f_0). \tag{48}$$

23

Then, as above,

$$X_+(f) = A \exp(i\theta) \, \delta(f-f_0) \, ,$$

$$x_+(t) = A \exp(i2\pi f_0 t + i\theta)$$

$$= A \cos(2\pi f_0 t + \theta) + i \, A \sin(2\pi f_0 t + \theta) \, . \tag{49}$$

Thus, the Hilbert transform of $x(t)$ in (47) is the sine component.

The procedure above succeeded because we completely eliminated the negative-frequency components of (48). However, suppose we compute the spectrum from a weighted time-limited segment of $x(t)$ in (47). Thus:

$$y(t) = w(t)x(t) \, ,$$

$$Y(f) = W(f) \circledast X(f) \, ,$$

$$= \frac{A}{2} \exp(i\theta) \, W(f-f_0) + \frac{A}{2} \exp(-i\theta) \, W(f+f_0) \, , \tag{50}$$

where weighting $w(t)$ satisfies (1). Figure 19 illustrates spillover of the negative- and positive-frequency components across the $f = 0$ border. This spillover can be controlled by choosing a window $W(f)$ with low near-by sidelobes and rapid decay of distant sidelobes. Then, if Lf_0 is large enough, when we multiply $Y(f)$ by $1 + \text{sgn}(f)$ to yield $Z(f)$, there will be little distortion from the desired function

$$D(f) = A \exp(i\theta) \, W(f-f_0) \quad \text{for all } f \, ;$$

$$d(t) = A \exp(i2\pi f_0 t + i\theta) \, w(t) \, . \tag{51}$$

We can then inverse Fourier transform $Z(f)$ to yield $z(t)$, and then *divide* $z(t)$ by weighting $w(t)$, in an attempt to approximate analytic waveform $x_+(t)$. This method will succeed in the interior region of the particular segment of the real data waveform selected, but will be in error near the edges of the segment because the neighboring data points (outside the selected segment) were never accounted for. This insufficiency can be alleviated by using tapered temporal weighting and (say) 50% overlapped segments, but retaining only the central 50% of the output data points of each segment, after the processing indicated above is carried out. How successful the technique is depends critically on Lf_0 and the window $W(f)$.

For a discrete-time waveform, the considerations are similar to those presented above, except that we now employ the discrete multiplicative window (46) (instead of $1 + \text{sgn}(f)$), and that Nyquist frequency $(2\Delta)^{-1}$ must also be considered, in addition to zero frequency, in terms of spillover. The procedure to be investigated is as follows: a long real data sequence $\{x_n\}$ is broken up into segments of length N, where adjacent segments overlap by 50%. Temporal weighting $\{w_n\}_0^{N-1}$ is multiplicatively applied to the N data points of a segment, and an N-point DFT is

taken of this product sequence. Sequence $\{u_n\}_0^{N-1}$ in (46) is then applied multiplicatively to the complex DFT output. An inverse DFT of this product is evaluated, and the result divided by weighting $\{w_n\}_0^{N-1}$. Then only the interior 50% of these N complex values are retained, and the other 50% discarded. By then abutting values of adjacent segment outputs, we obtain the analytic waveform sequence corresponding to the original real data sequence $\{x_n\}$. Very long data sequences can be handled in this manner; only the extreme edges are subject to significant error.

If we look at some of the better windows presented earlier, for example figures 11, 12, and 15, we see that very deep sidelobes are realized and maintained for $|Lf|>4$. Thus for a sinusoid at frequency f_0, spillover is small in figure 19 if

$$\frac{4}{L} < f_0 < \frac{1}{2\Delta} - \frac{4}{L} ; \tag{52}$$

the upper bound is due to spillover at the Nyquist frequency. Since segment length L is composed of N data points, (52) can be expressed as

$$\frac{4}{N} < f_0\Delta < \frac{1}{2} - \frac{4}{N} . \tag{53}$$

For example, a 1024-point DFT yields

$$.004 < f_0\Delta < .496 . \tag{54}$$

Thus, the majority of frequency components in sequence $\{x_n\}$ are capable of very accurate Hilbert transformation. To widen the bounds in (52), we must increase L and decrease Δ. If Δ is chosen to minimize aliasing in the first place, the only recourse is to increase N, the number of points in each data segment. Thus, larger-size DFTs should perform better in terms of lower error of the DHT and lower allowed frequencies in the given sequence $\{x_n\}$.
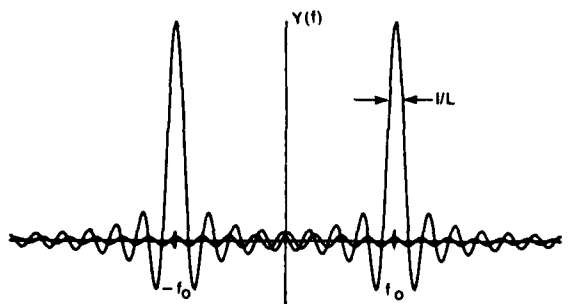

Figure 19. Spectrum of Weighted Time-Limited Segment of x(t)

25

SIMULATION RESULTS

The fifteen weightings given earlier are summarized in table 2. They have been tried as candidates for the DHT technique presented in the previous section. Input signals composed of real unit-amplitude pure tones at several different frequencies and phases have been used to test the accuracy of the DHT technique. In particular, tone frequencies f_0, taking the four values

$$f_0\Delta = \{\sqrt{2}/5, \quad \sqrt{2}/27, \quad \sqrt{2}/65, \quad \sqrt{2}/350\} = \{.283, \quad .052, \quad .022, \quad .004\} \quad (55)$$

were selected. (The square root was used to avoid taking synchronized periodic samples of the input waveform. It was found that samples synchronized with the tone frequency, such as $f_0\Delta = .25$, gave inordinately small errors.) The phases of each tone were taken as 0 and $-\pi/2$ corresponding to a cosine and sine waveform, respectively. Intermediate-phase tones are available as linear combinations of these two cases.

Table 2. Window Characteristics

Weighting	Peak Sidelobe (dB)	Asymptotic Decay (dB/octave)
1. Hanning	-31.47	18
2. Blackman	-58.11	18
3. Exact Blackman	-68.24	6
4. "Minimum" 3-Term	-70.83	6
5. 3-Term	-62.05	6
6. "Minimum" 4-Term	-92.01	6
7. 4-Term	-74.39	6
8. 3-Term with Continuous Third Derivative	-46.74	30
9. 3-Term with Continuous First Derivative	-64.19	18
10. 4-Term with Continuous Fifth Derivative	-60.95	42
11. 4-Term with Continuous Third Derivative	-82.60	30
12. 4-Term with Continuous First Derivative	-93.32	18
13. Hamming	-43.19	6
14. Minimum 3-Term	-71.48	6
15. Minimum 4-Term	-98.17	6

Since the Hilbert transform of a cosine with arbitrary phase is a sine of the same phase (see (49)), we can compute the error of the DHT technique very easily for pure tones. For the retained interior 50% output data points of each segment, four error measures were evaluated. They were the maximum magnitude-error and the average magnitude-error for both the real and imaginary parts of the analytic waveform sequence. The two error measures (maximum and average) for the real part were virtually zero, because of the trigonometric function error and the round-off noise of the 12-digit calculator employed. The average magnitude-error measure for the imaginary part of the analytic sequence, i.e., the error of the discrete Hilbert transform, is presented in tables 3-6 for the four tone frequencies listed in (55). A program for the DHT technique and the error calculation is presented in the appendix.

The first fact to observe from tables 3-6 is that the quality of the DHT varies greatly with the window. In fact, the ratio of errors can become as large as 300,000 when we consider different windows for a specified waveform. In order to present the numerical values more conveniently for comparison, the errors have been scaled by 10^9 in tables 3-5 and by 10^6 in table 6. Thus, some of the errors listed in tables 3-6 are small indeed.

The maximum magnitude-error, for all the input frequencies, phases, and windows considered, was approximately 4-to-6 times larger than the average magnitude-error. (It has not been tabulated here, in order to save space.)

When the data frequency, f_0, is near the center of the zero-to-Nyquist frequency band, the best windows are observed from tables 2 and 3 to be those for which the asymptotic decay is 18 dB/octave or better. This holds regardless of the size of the near-by sidelobes. Even the window in figure 15, with a peak sidelobe less than -98 dB, does not perform as well as the Hanning window which has a -31.5 dB sidelobe; in fact, the error is about 70 times larger. This numerical result is consistent with the discussion surrounding figure 19 — we have virtually eliminated spillover across the $f = 0$ and $f = .5/\Delta$ borders by using rapidly decaying windows, when $f_0 \sim .25/\Delta$.

When the frequency, f_0, is lowered to one-tenth of the Nyquist frequency, the best windows are those with decays of 30 dB/octave or better; see table 4. This trend continues in table 5 for f_0 equal to 0.044 of the Nyquist frequency, where the sole window with a 42 dB/octave decay is observed to be best.

However, when data frequency, f_0, approaches the bounds of (53), a different ordering of windows is observed; see table 6). Now the windows with the deepest near-by sidelobes (cases 6 and 15 in table 2) have the least error, although the range of errors in table 6 are less pronounced than those in the previous tables. Thus, the best weighting $w(t)$ to employ depends on the spectrum of the data sequence $\{x_n\}$ that we are subjecting to the DHT. A compromise between deep near-by sidelobes and fast asymptotic decay must be accepted for a waveform occupying most of the zero-to-Nyquist frequency band. For example, the average magnitude-errors for the minimum 4-term window of figure 15 are approximately

$$.5E-6, \quad 1.6E-6, \quad 2.6E-6, \quad 6.3E-6 \tag{56}$$

for the four frequencies considered in tables 3-6. This is a very small error and indicates that the proposed DHT technique has considerable merit, provided the weighting in (50) is chosen appropriately.

Other waveforms were simulated and subjected to the DHT and error analysis. They included narrow-band waveforms, high-frequency tones (near Nyquist), and other phases than 0 and $-\pi/2$. No surprises were encountered; results were consistent with those already presented above. Also a simple Gaussian weighting with several different standard deviations was tried; the best Gaussian weighting occured when it was set equal to .0053 at the segment edges and .27 at the edges of the retained points. Although the error of the DHT could be made to be very good for tone frequencies well-removed from zero and Nyquist frequency, it was poorer for frequencies fairly near zero and Nyquist; the worst error was 1.36E-4 at $f_0\Delta = 0.044$, which is 20 times worse than can be realized with weighting 15 in table 6. This

is due to the spillover caused by the wide mainlobe of the Gaussian window when the effective duration of the weighting is chosen narrower than the segment length.

Table 3. Average Magnitude-Error for $f_0\Delta = \sqrt{2}/5 = .283$

Weighting	Error $\times$ 10^9 for	
	Cosine	Sine
1	2.83	8.52
2	1.89	4.18
3	6050.	7470.
4	4350.	5370.
5	10500.	12900.
6	70.4	86.4
7	2090.	2580.
8	1.38	1.45
9	1.75	3.47
10	1.38	1.45
11	1.38	1.45
12	1.41	1.72
13	52400.	64700.
14	4700.	5810.
15	415.	512.

Table 4. Average Magnitude-Error for $f_0\Delta = \sqrt{2}/27 = .052$

Weighting	Error $\times$ 10^9 for	
	Cosine	Sine
1	305.	454.
2	138.	206.
3	16300.	24400.
4	11700.	17500.
5	28200.	42300.
6	164.	245.
7	5580.	8360.
8	.56	.77
9	108.	161.
10	.23	.23
11	.37	.48
12	24.3	36.2
13	142000.	213000.
14	12700.	19000.
15	1090.	1630.

Table 5. Average Magnitude-Error for $f_0\Delta = \sqrt{2}/65 = .022$

Weighting	Error × 10⁹ for	
	Cosine	Sine
1	4360.	6020.
2	1950.	2700.
3	33100.	45800.
4	23300.	32200.
5	58000.	80300.
6	61.1	52.0
7	10700.	14900.
8	39.5	54.3
9	1520.	2110.
10	.93	1.27
11	20.4	28.1
12	326.	452.
13	300000.	416000.
14	25300.	35100.
15	1890.	2620.

Table 6. Average Magnitude-Error for $f_0\Delta = \sqrt{2}/350 = .004$

Weighting	Error × 10⁶ for	
	Cosine	Sine
1	495.	501.
2	154.	86.1
3	24.0	50.6
4	45.2	50.5
5	61.5	129.
6	7.01	7.27
7	29.3	15.4
8	132.	241.
9	95.4	45.6
10	189.	398.
11	34.0	70.6
12	9.07	15.3
13	899.	429.
14	41.	53.3
15	3.71	6.31

SUMMARY

When strong interference, either tonal or narrowband, occurs additively with a desired signal, its effect on frequencies removed from the interference band can be greatly reduced by using windows with low sidelobes and significant decay of the sidelobes. Thus close-by interference rejection requires the immediate sidelobe region of the window to be small, while distant interference rejection requires a rapidly-decaying sidelobe response. The type of windows considered here furnish several alternative choices, depending on the application of interest, and range from -31 dB to -98 dB for the peak sidelobe, or 6 dB/octave to 42 dB/octave for the asymptotic decay. The weighting given by (3) is non-negative for all the numerical coefficients listed here.

Use of some of these windows in a proposed discrete Hilbert transform technique yields very small errors over a wide range of frequency components of the given data sequence, provided that 50% overlapped processing is employed. Two DFTs are necessary per segment, and the edge 50% of the output values of each segment must be discarded. Larger-size DFTs yield less error, especially for frequencies near the bounds in (53), but they require more storage.

REFERENCES

1. F. J. Harris, "On the Use of Windows for Harmonic Analysis with the Discrete Fourier Transform," *Proc. IEEE*, Vol. 66, no. 1, Jan. 1978, pp. 51-83.

2. A. V. Oppenheim and R. W. Schafer, *Digital Signal Processing*, Prentice-Hall Inc., N.J., 1975.

Appendix

PROGRAM FOR DISCRETE HILBERT TRANSFORM

The subroutine for the DHT technique described earlier is contained in lines 660-820 of the program listed below in table A-1. The remainder of the program contains the data creation, the weightings in lines 100-240, the error calculation, and a DFT in the subroutine beginning with line 830. On input to the DHT subroutine call in line 500, array X contains the N-point data segment to be Hilbert transformed, and array Y is zero. On output from the DHT subroutine call, elements N/4 to 3N/4 of arrays X and Y contain the central half of the original data segment and its DHT, respectively.

Table A-1. Program for Discrete Hilbert Transform

```
10      F0del=SQR(2)/5          ! 5,27,65,350
20      Phase=-PI/2
30      N=1024                  ! SIZE OF FFT
40      PRINTER IS 0
50      PRINT "F0del =";F0del,"Phase =";Phase,"N =";N
60      PRINT
70      OPTION BASE 1
80      DIM X(1024),Y(1024),C(1024),S(1024),W(1024)
90      DIM H(0:59),A(0:3)
100     DATA .5,.5,0,0
110     DATA .42,.5,.08,0
120     DATA .42659,.49656,.07685,0
130     DATA .42323,.49755,.07922,0
140     DATA .44959,.49364,.05677,0
150     DATA .35875,.48829,.14128,.01168
160     DATA .40217,.49703,.09892,.00188
170     DATA .375,.5,.125,0
180     DATA .40897,.5,.09103,0
190     DATA .3125,.46875,.1875,.03125
200     DATA .338946,.481973,.161054,.018027
210     DATA .355768,.487396,.144232,.012604
220     DATA .53836,.46164,0,0
230     DATA .4243801,.4973406,.0782793,0
240     DATA .3635819,.4891775,.1365995,.010641:1
250     READ H(*)
260     T=2*PI*F0del
270     FOR K=1 TO N
280     B=T*K+Phase
290     C(K)=COS(B)
300     S(K)=SIN(B)
310     NEXT K
320     FOR Nc=1 TO 15
330     FOR L=0 TO 3
340     A(L)=H(L+4*(Nc-1))
350     NEXT L
360     PRINT "(";Nc;")";A(0);A(1);A(2);A(3)
370     A(1)=-A(1)
```

31

```
380     A(3)=-A(3)
390     T=2*PI/(N+1)
400     FOR K=1 TO N
410     B=T*K
420     S=A(0)
430     FOR L=1 TO 3
440     S=S+A(L)*COS(L*B)
450     NEXT L
460     W(K)=S
470     NEXT K
480     MAT X=C
490     MAT Y=ZER
500     CALL Dht(N,X(*),Y(*),W(*))
510     Mr=Mi=Ar=Ai=0
520     FOR K=N/4 TO 3*N/4
530     Dr=ABS(C(K)-X(K))
540     Di=ABS(S(K)-Y(K))
550     Mr=MAX(Mr,Dr)
560     Mi=MAX(Mi,Di)
570     Ar=Ar+Dr
580     Ai=Ai+Di
590     NEXT K
600     PRINT Mr,Mi,Ar/(.5*N+1),Ai/(.5*N+1)
610     PRINT
620     NEXT Nc
630     PRINT LIN(3)
640     PRINTER IS 16
650     END
660     SUB Dht(N,X(*),Y(*),W(*))          DISCRETE HILBERT TRANSFORM
670     MAT X=X.W
680     CALL Fft10(N,X(*),Y(*))
690     FOR K=2 TO N/2
700     X(K)=X(K)*2
710     Y(K)=-Y(K)*2
720     NEXT K
730     FOR K=N/2+2 TO N
740     X(K)=Y(K)=0
750     NEXT K
760     CALL Fft10(N,X(*),Y(*))
770     FOR K=N/4 TO 3*N/4
780     T=1/(W(K)*N)
790     X(K)=X(K)*T
800     Y(K)=-Y(K)*T
810     NEXT K
820     SUBEND
830     SUB Fft10(N,X(*),Y(*))     ! N <= 2^10 = 1024, N=2^INTEGER
```

Initial Distribution List

ADDRESSEE	NO. OF COPIES
ASN (RE&S) (D. E. Mann)	1
OUSDR&E (W. J. Perry)	1
Dep. USDR&E (Res & Adv Tech) (R. M. Davis)	1
Dep. USDR&E (Dir Elect & Phys Sc) (L. Wiseberg)	1
OASN, Spec Dep for Adv Concept (Dr. D. Hyde)	1
OASN, Dep Assist Sec (Res & Adv Tech.) (Dr. R. Hoglund)	1
ONR (Code ONR-100, -200, -102, -480, -212, -222, -230, -486, -431)	9
CNO (OP-090, -902, -951, -953, -96)	5
CNM (MAT-00, -08T, -08T2, SP-20, -ASW-122)	5
DIA (DT-2C)	1
NRL	1
NRL, USRD	1
NORDA (Code 110) (Dr. R. Goodman)	1
USOC (Code 240)	1
OCEANAV	1
NAVOCEANO (Code 00, 02)	2
NAVELECSYSCOM (ELEX 03, PME-124)	2
NAVSEASYSCOM (SEA-003, -06R, -996)	3
NOSC (Code 00, Code 6565)	2
DTNSRDC	1
NAVCOASTSYSLAB	1
NISC	1
NAVPGSCOL	1
Center for Naval Analysis (Acq. Unit)	1
DTIC	12
DARPA	1
National Research Council	1